Journal of Manufacturing Processes 56 (2020) 1136–1145

Contents lists available at ScienceDirect

Journal of Manufacturing Processes

journal homepage: www.elsevier.com/locate/manpro

Weld morphology and mechanical properties in laser spot welding of quenching and partitioning 980 steel

Wei Zhang[a,b], Shanglu Yang[c,d,*], Zhe Lin[c], Wu Tao[c]

[a] Changchun Institute of Optics, Fine Mechanics and Physics, Chinese Academy of Sciences, Changchun, 130033, China
[b] University of Chinese Academy of Sciences, Beijing, 100049, China
[c] Shanghai Institute of Optics and Fine Mechanics, Chinese Academy of Sciences, Shanghai, 201800, China
[d] Center of Materials Science and Optoelectronics Engineering, University of Chinese Academy of Sciences, Beijing, 100049, China

ARTICLE INFO

Keywords:
Quenching and partitioning steels
Laser spot welding
Real-time modulating focus position
Resistance spot welding
Weld nugget size
Tensile shear strength

ABSTRACT

Quenching and partitioning (QP) steels offer excellent mechanical properties, which have shown a promise to reduce the vehicle weight and improve fuel economy. One of the bottlenecks for their applications in the automotive industry is the poor weldability. Laser spot welding (LSW) process was proposed in this study to join them in a lap joint configuration. It was found that the weld nugget size of laser spot welds was limited with fixed focus position due to the instability of laser beam energy. A novel method of laser spot welding process with real-time modulating the focus position was developed. Using the newly developed LSW process can significantly enlarge the weld diameter from 5.53 mm to 7.10 mm and improve the weld strength from 15.08 kN to 24.61 kN. The improvement in the weld diameter and the weld strength were attributed to increase in the irradiated area, which reduces the laser beam intensity and the materials loss. In addition, a high-speed camera was used to real-time monitor the laser spot welding process. Furthermore, the welds produced by newly developed laser spot welding process can generate the weld strength higher than RSW welds.

1. Introduction

Advanced high strength steels (AHSSs) have been widely used in the automotive industry to reduce vehicle weight and improve fuel economy [1]. Compared with first and second generation AHSSs, third generation AHSSs not only provide good formability but also save cost. Speer et al. [2] proposed a novel quenching and partitioning process to produce a new type of third generation steels having superior strength and ductility, named as QP steels. Considering advantages of QP steels over traditional AHSSs, the automotive industry has shown intensive interest in applying them in the body structure. Before QP steels are implemented in a vehicle, their weldability has to be evaluated.

Currently, resistance spot welding (RSW) still is the primary joining solution for the automotive industry [3]. There are typically 3000–5000 RSW welds in an assembled vehicle [4]. Liu et al. [5] developed a double pulse RSW method to enhance the tensile-shear strength of QP980 steels with a desirable failure mode. Russo et al. [6] used RSW process to weld galvanized QP and TRIP steels and study the effects of the welding parameters on corrosion behavior and the weld strength of the spot welds. It was found that welding time and current have the primary effect on the weld strength and the electrode force has beneficial influence on the corrosion performance. Besides, the loss of metal during expulsion leads to the formation of the weld defects such as voids and porosity, which reduce the peak load of the welds [7].

Compared to resistance spot welding, laser welding is a single-sided joining process, which provides faster welding speed, lower heat input and higher manufacturing flexibility. Considering the advantages of laser welding over RSW, many efforts had been spent in using laser welding process to join AHSSs. Sharma and Molian [8] used an Yb:YAG disk laser to study the weldability of TRIP 780, DP980, USIBOR and mild steels in a butt joint configuration. Yang et al. developed different approaches including GTAW-assisted laser welding [9], oxygen-assisted laser welding [10] and semi-cutting assisted laser welding [11] techniques in order to weld zinc coated steels in a gap-free lap joint configuration. Experimental results shown that the developed approaches can suppress highly-pressurized zinc vapor and achieved high-quality welds without removing the zinc coating at the interface of two sheets.

Except linear laser beam welding, laser spot welding (LSW) has also been developed to join different types of materials. Yang et al. [12] developed a laser spot welding technique with continuous CO_2 laser beam to spot weld low carbon steel, that has the yield strength of 320 MPa. It was found that the tensile strength of the spot welds mainly

* Corresponding author at: Shanghai Institute of Optics and Fine Mechanics, Chinese Academy of Sciences, Shanghai, 201800, China.
E-mail address: yangshanglu_lab@126.com (S. Yang).

https://doi.org/10.1016/j.jmapro.2020.05.057
Received 4 February 2020; Received in revised form 25 May 2020; Accepted 31 May 2020

Table 1
Chemical compositions and mechanical properties of QP980 steel.

C	Mn	Si	Al	S	P	Fe	YS/MPa	UTS/MPa	Elongation/%
0.24	1.97	1.41	0.04	< 0.01	< 0.02	Bal.	618	1037	20

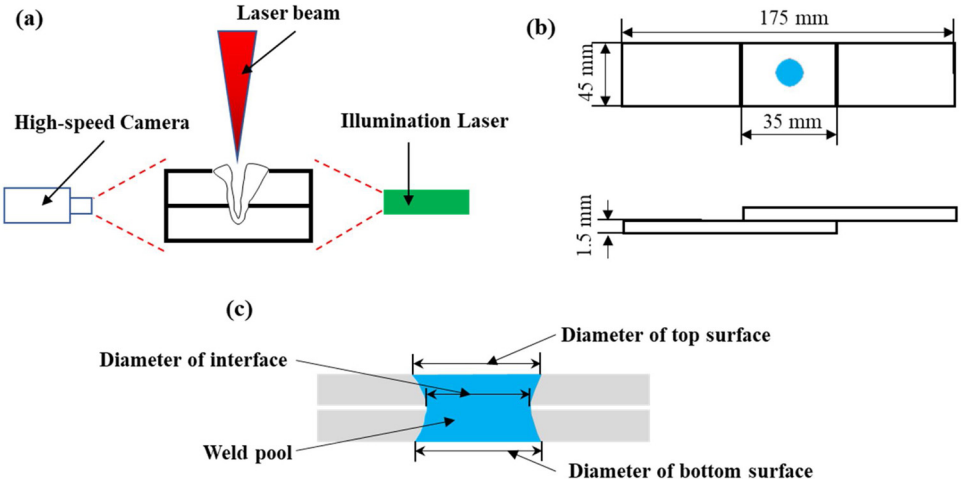

Fig. 1. Schematic diagram of (a) experimental setup; (b) tensile-shear test sample and (c) the defined weld diameters.

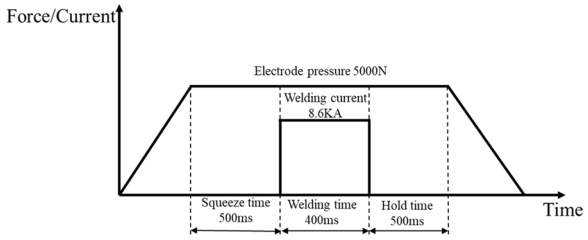

Fig. 2. Welding schedule of resistance spot welding.

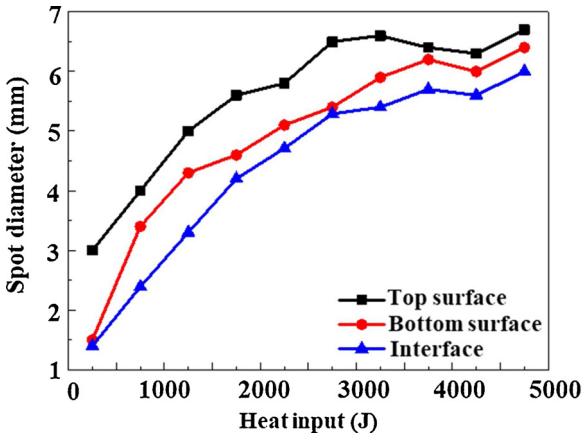

Fig. 3. Effect of heat input on the weld diameters of the top surface, the interface and the bottom of the weld.

depended on the joined area and the maximum weld diameter. Kaplan et al. [13] developed a keyhole laser spot welding process to join different types of materials, including A1050, A5083, pure Ti, Ti-6Al-4 V, carbon steel and SUS 304. As stated by Kaplan et al. [13], the beam power, spot diameter and pulse duration have significant influences on the weld shape formation. Furthermore, optimizing the pulse duration and pulse profile can suppress the formation of cracks, craters and pores in the spot weld. In addition, the circular LSW joints failed with a "plug type" of failure mode under "peel-coach" loading condition [14]. Daneshpour et al. [15] joined dual phase 780 steel and deep drawing steel (DC04) by LSW and RSW. According to Daneshpour et al. [15], laser spot welds and resistance spot welds have different fatigue performance under the cyclic loads at "high load" and "low load" levels. The effective laser pulse energy played the primary influence on the tensile shear strength of circular laser spot welds in low carbon steel [16]. There are three types of failure modes for the circular laser spot welds: (a) interfacial; (b) desired pullout failure mode; (c) undesired pullout failure mode. Among these three types of failure modes, the desired pullout failure mode corresponded to the maximum tensile shear strength. Furthermore, it was found that excessive energy input will lead to the formation of expulsion, which directly reduced the peak load of the tensile shear strength.

Shanmugam et al. [17] applied an Nd: YAG laser to laser spot weld SUS 304 steel. When changing laser beam from a straight beam to titled laser beam, the weld shape turned from almost circle to elliptic. In addition, the weld penetration depth and the bead width were decreased by decrease in the incident angle from 85° to 75°. Alizadeh-Sh et al. [18] studied metallurgical and mechanical properties of circular laser spot weld in AISI 304 L steel. According to Alizadeh-Sh et al. [18], the grain growth in heat affected zone (HAZ) led to its softening and the mechanical properties of circular laser spot weld in AISI 304 L steel were mainly determined by fusion zone area and HAZ softening level. Miyagi et al. [19] used X-ray phase contrast technique to study the crack propagation and porosity formation during laser spot welding of A1050, A2024, A5083 and A 6061. It was found that hot cracking mainly located in the center of laser spot weld, which initiated within the weld and propagated toward the upper surface of laser spot weld under the weld stress. In addition, Zhang and Cao [20] developed a temporal laser pulse shaping method to suppress the weld defects in laser spot welds in AZ31 magnesium alloy. Although many progress on LSW has been made, low weld strength caused by undesirable melt pool is still a big challenge for their practical applications. Meanwhile, laser beam energy absorption by the molten pool and laser-induced plasma behavior were still not well understood. There is little open literature about using laser spot welding process to join third generation steels.

In this paper, a novel laser spot welding process of real-time modulating the laser focus position was developed to join QP980 steel, which was completely different from conventional laser spot welding

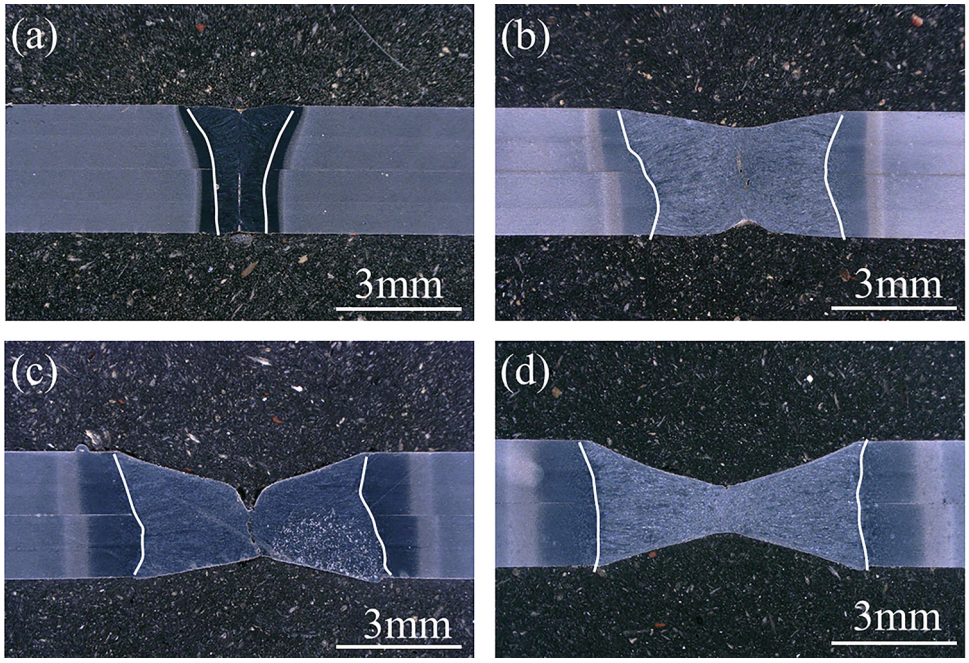

Fig. 4. Cross-section views of the laser spot welds obtained by conventional LSW with different heat input: (a) 250 J; (b) 1750 J; (c) 3250 J; (d) 4750 J.

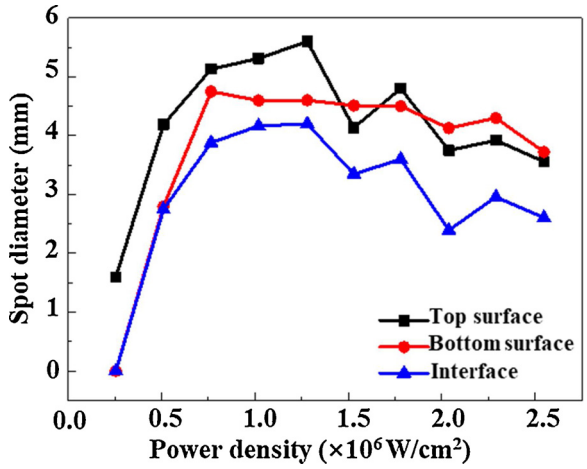

Fig. 5. Effect of laser beam energy density on the weld diameters of the top surface, the interface and the bottom of the weld. Heat input was fixed as 1750 J.

with a fixed focus position. The weld nugget diameter and tensile shear strength were used as a standard to assess the weld performance. A high-speed camera was applied to real-time monitor the dynamic behaviors of laser-induced plasma and plume. In addition, resistance spot welding process was also conducted to join QP steels in order to compare the mechanical performance of LSW and RSW welds.

2. Experimental setup

1.5 mm thick QP980 steel sheets provided by Anshan Iron & Steel Co., Ltd. were used in this study. The nominal chemical compositions along with the typical yield strength, ultimate tensile strength (UTS) and elongation are summarized in Table 1.

IPG PHOTONICS YLS-10,000 fiber laser was used to perform LSW experiments. Its wavelength is 1070 nm and the maximum output power is 10 kW. Laser beam was delivered to a welding head (HIGHYAG BIMO) using an optical fiber with the core diameter of 200 μm. A high-precision 6-axis KUKA 60HA robot was used to control the laser head movement. The laser beam was vertically delivered on the workpieces with a 0.5 mm beam diameter on focal position using a 300 mm focusing lens. A high-speed camera (Photron FASTCAM) was introduced to real time record the laser-induced plasma and plume during LSW process. An illumination laser with 808 nm wavelength was applied for lighting the contrast of laser-induced plasma and plume. The laser-induced plasma and plume was captured in the parallel angle of the workpiece where the plasma located above top surface and below bottom surface can be observed. Schematic diagram of the experimental system was indicated in Fig. 1a. The two QP980 metal sheets were clamped tightly and assumed as a zero-gap. Two types of LSW experiments were carried out: a) laser beam spot was focused on the top surface of two metal sheets and not moved during the whole LSW process; b) laser beam spot was focused on the top surface of two metal sheets at the beginning of the LSW, then were moved toward/reverse to the incident direction of laser beam during LSW process to change the laser beam energy density.

The optical images of top and bottom surface of the LSW joints were obtained using a digital optical microscope (OM, KEYENCE VHX-6000). The cross-section of the LSW joints were prepared by standard procedure of electric spark cutting, mounting and mechanically polishing. Polished samples were etched using 4% nital regent and then characterized by OM. To achieve high quality images of the laser-induced plasma and plume, a 200K-M3 lens was installed on the camera, combined with an 808 nm optical filter. The optimized parameters were set as the shooting speed of 2000 fps and shutter speed of 1/80000 s. Tensile-shear tests were carried out at room temperature with the cross –head speed of 3 mm/min by a universal mechanical tester (SUNS Co., Ltd.). The tested sample geometry and the defined weld diameters on the top, at the interface and at the bottom of the weld are schematically shown in Fig. 1b and 1c. The tensile direction was parallel to the rolling direction of the experimental material. Three specimens were tested using the same welding parameters to obtain the average force value.

To compare the mechanical performance of LSW and RSW joints, a resistance spot welding machine with servo-gun was used to weld QP980 steel sheets similar to the selected materials used in LSW process, which provides a stable direct current (DC) with a medium frequency of 1000 Hz. The welding schedule is shown in Fig. 2.

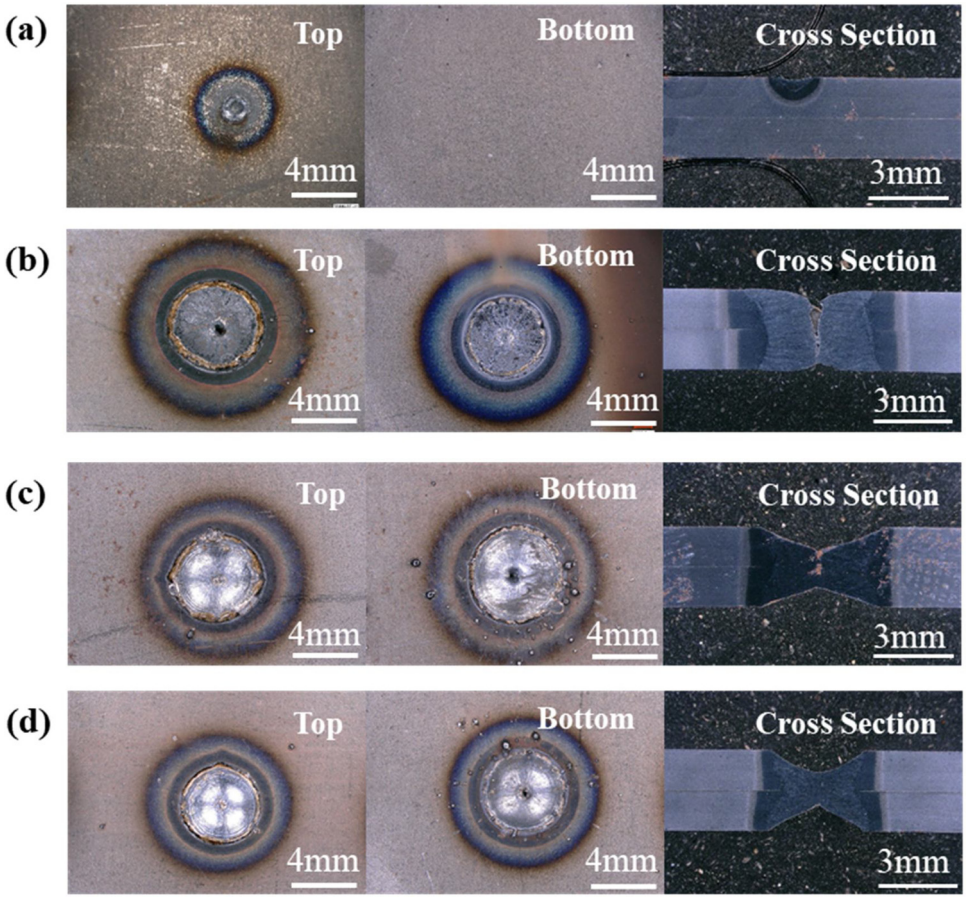

Fig. 6. Morphology of the laser spot welds obtained by conventional LSW with different power density: (a) $0.26 \times 10^6 W/cm^2$; (b) $0.77 \times 10^6 W/cm^2$; (c) $1.78 \times 10^6 W/cm^2$; (d) $2.55 \times 10^6 W/cm^2$.

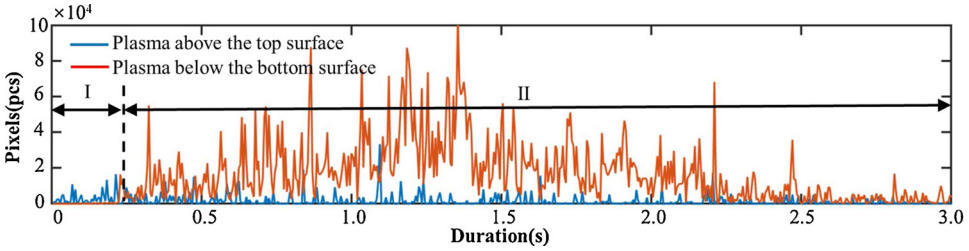

Fig. 7. The varying pixels of laser-induced plasma and plume for conventional LSW process.

3. Results and discussion

3.1. Effect of laser spot welding parameters on the weld morphology

Effect of heat input on the weld morphology were firstly investigated. The heat input Q is defined as $Q = P \times t$ where P is the laser power and t is the welding duration. In addition, the laser power and laser beam diameter were kept constant by 2500 W and 0.5 mm, respectively. And the laser beam energy density equals to 1.27×10^6 W/cm^2. The heat input was only adjusted by varying the welding duration. As shown in Fig. 3, the weld diameters on the top surface, at the interface and at the bottom of the spots were increased rapidly with increase in heat input. When heat input was larger than 2750 J with the weld duration of 1.1 s, however, change in the weld diameters tends to be gentle. This phenomena indicated that the maximum weld nugget diameter has been reached to its threshold. In addition, the weld diameter at the interface of the weld was always smaller than those on the top and at the bottom of the weld.

Fig. 4 shows that the weld morphology varied with different heat input. The weld penetration depth was through the bottom of the metal sheets even by a small heat input of 250 J where a "Y-shape" weld morphology was represented. When heat input was increased above 1750 J, a "X-shape" weld morphology and a crater in the weld center were observed. The more the heat input, the deeper the crater size it was. It's well known that the collapse will lead to reduce in mechanical property. Experimental results in Fig. 3 demonstrated that simply modulating heat input can't produce a desired large weld diameter and high-quality weld.

The effect of laser beam energy density on the weld morphology were further studied. Here, heat input was fixed as 1750 J, which can produce a spot weld with small crater on the top surface of the weld. As shown in Fig. 5, there existed a maximum weld diameter when the laser beam energy density was $1.27 \times 10^6 W/cm^2$. Further increase in the laser beam energy density led to significantly decrease in the weld diameters, from 4.10 mm interface diameter with laser beam energy density of $1.27 \times 10^6 W/cm^2$ to 2.75 mm with laser beam energy density of

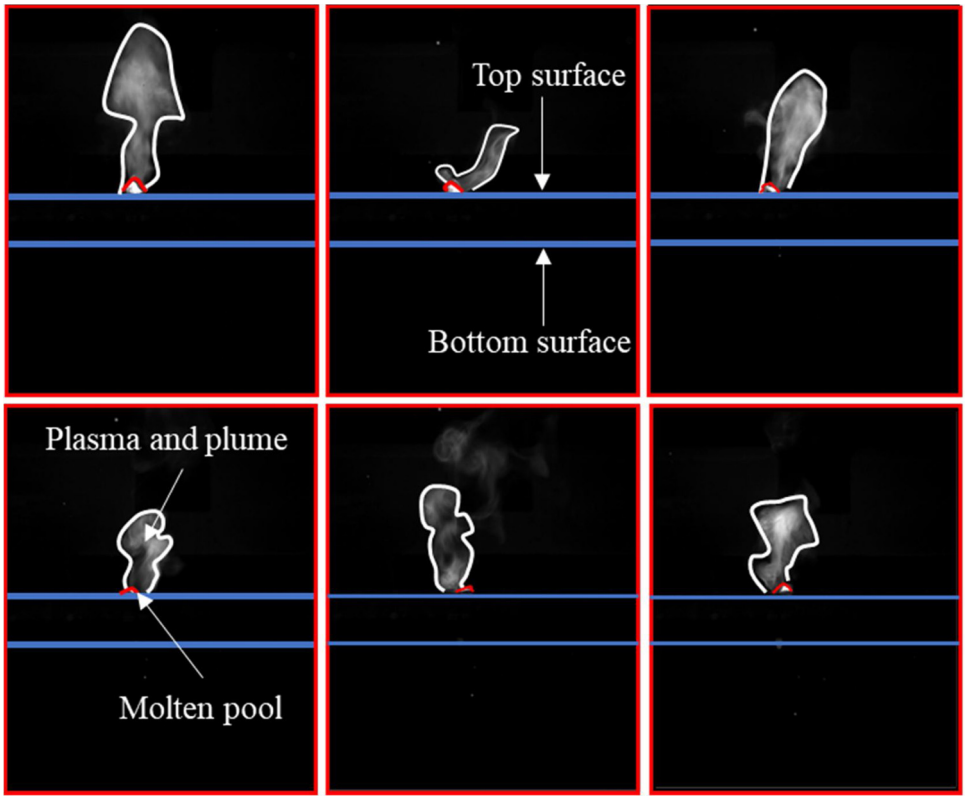

Fig. 8. Time-dependent plasma behavior using conventional LSW before laser beam fully penetrated through the metal sheets.

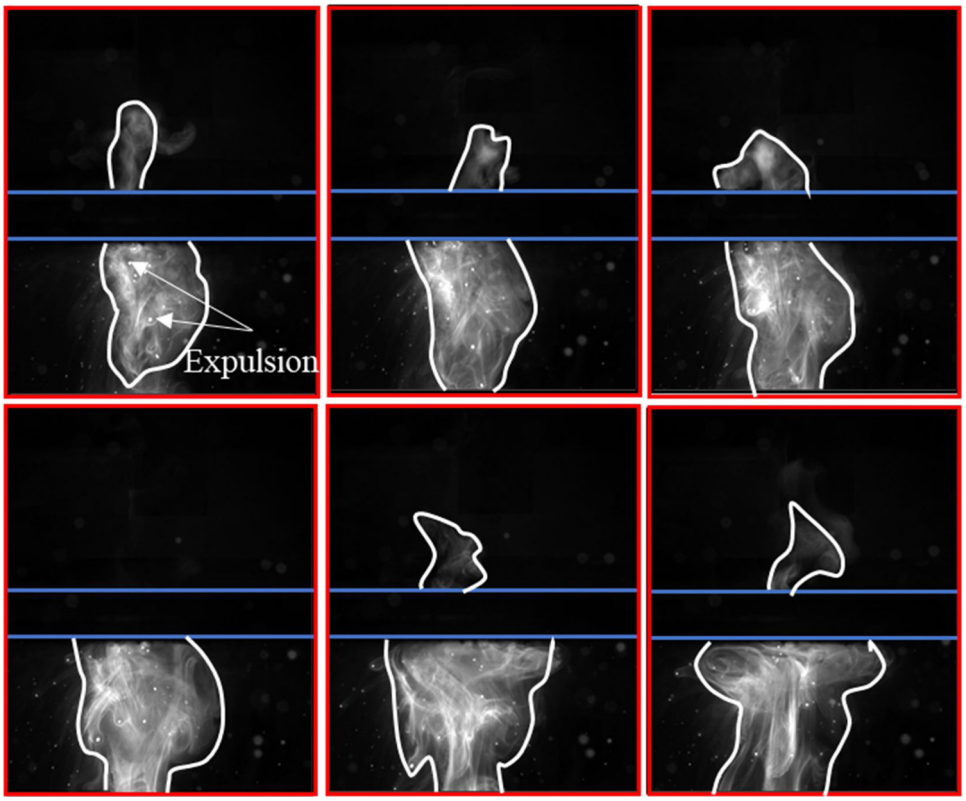

Fig. 9. Time-dependent plasma behavior using conventional LSW after laser beam fully penetrated through the two metal sheets.

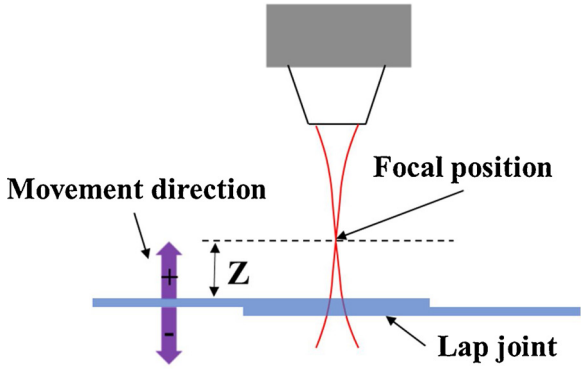

Fig. 10. Schematic diagram of novel LSW process.

Table 2
Movement distance, moving velocity and the welding duration of novel LSW process.

Sample	Z/mm	Moving velocity/mm·s^{-1}	Welding duration/s
1	−10	10	1
2	−20	10	2
3	−30	10	3
4	+10	10	1
5	+20	10	2
6	+30	10	3

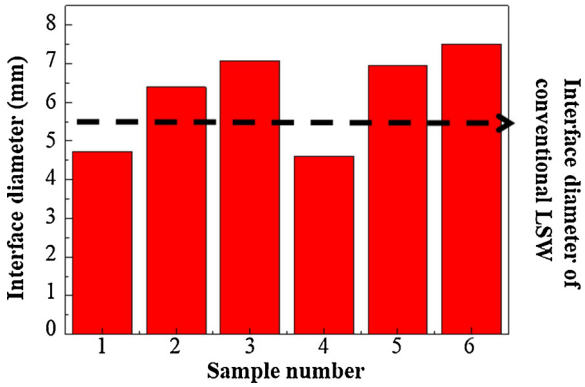

Fig. 11. The weld diameters obtained under different movement conditions.

2.55×10^6W/cm^2.

Fig. 6 shows the top, bottom and cross-section views of the typical welds, which were obtained with different laser beam energy density. When laser beam energy density was 0.26×10^6W/cm^2, the laser beam only melt the top metal sheet. Increase in the laser beam energy density led to a full penetration weld. In addition, concave in the weld center was observed due to the shrinkage during the solidification process. When laser beam energy density was further increased to 1.78×10^6W/cm^2 and 2.55×10^6W/cm^2, the weld diameters were significantly decreased together with a deep crater appeared on both sides of the weld center as shown in Fig. 6c and 6d. Furthermore, a large amount of expulsion was produced in the bottom surface of the weld. The deep crater formation in the weld center could be attributed to the strong effect of recoil pressure by intensive laser beam energy intensity. Under strong recoil pressure from the high laser beam density, a large amount of the liquid metal was ejected out of the molten pool as expulsion because the surface tension failed to balance it. Furthermore, most of laser beam energy is lost due to fully penetrated through the metal sheets and only portion of laser beam energy is absorbed by the metal sheets. As a result, small weld diameter was generated with appearance of a crater at the weld center even with high laser beam energy density.

3.2. Dynamic behaviors of laser-induced plasma and plume during conventional LSW process

In order to study dynamic behaviors of laser-induced plasma and plume, a high speed camera was used to real-time monitor the laser spot welding process. According to different brightness values, the number of pixels of laser-induced plasma and plume was extracted by Matlab software as shown in Fig. 7. Besides, the plasma area is proportional to the number of pixels. By analyzing the variation in the plasma area above the top surface and below the bottom surface, the LSW process can be classified by two phases based on their features: (I) before laser beam fully penetrated through the two metal sheets; (II) after laser beam fully penetrated through the bottom of the metal sheets.

Before laser beam fully penetrated through the metal sheets, the LSW process is likely a drilling process. Fig. 8 shows the successive 6 pictures extracted from the recorded images of the LSW process before laser beam fully penetrated through the metal sheets. As shown in Fig. 8, under the intensive evaporation, portion of liquid metal was ejected out of the molten pool. Furthermore, the molten pool seriously fluctuates around the laser beam. The shape and size of laser-induced plasma and plume were also varied over time. After the laser beam fully penetrated through the two metal sheets in Fig. 9, a large amount of liquid metal are ejected from the bottom of the metal sheets because the surface tension of the molten pool is smaller than the recoil pressure force coming from the laser beam. The liquid metal is continuously and randomly ejected along different directions. More importantly, the laser-induced plasma and plume below the bottom of the metal sheets has a larger size than that above the top surface of two metal sheets. This phemomena indicates that most of laser beam energy is lost after laser beam fully penetrated the metal sheets, resulting in small weld diameter.

3.3. Development of a novel LSW process

Based on the analysis of the weld pool formation and laser-induced plasma and plume dynamic behaviors taking place during conventional LSW process, a novel LSW technique was proposed in this study to join QP steels. The focal position of laser beam was moved from the top surface of the metal sheets to a specific position away along or inverse to the laser beam propagation direction. The schematic diagram of this

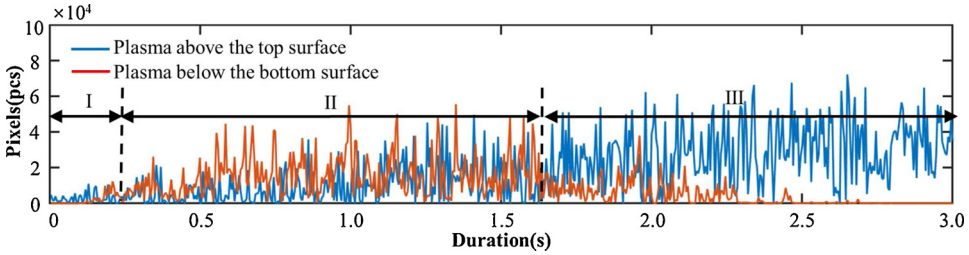

Fig. 12. The varying pixels of laser-induced plasma and plume for novel LSW process.

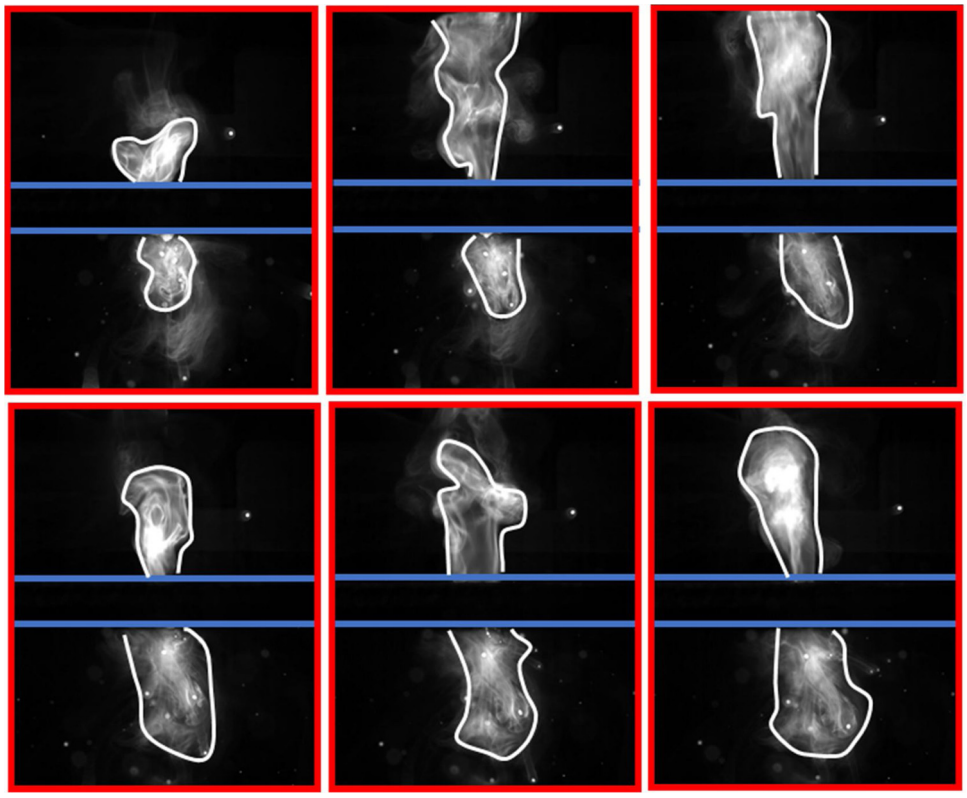

Fig. 13. Time-dependent laser-indcued plasma behaviors using novel LSW when laser beam fully penetrated through the metal sheets. This corresponds to sample 6 in Table 2.

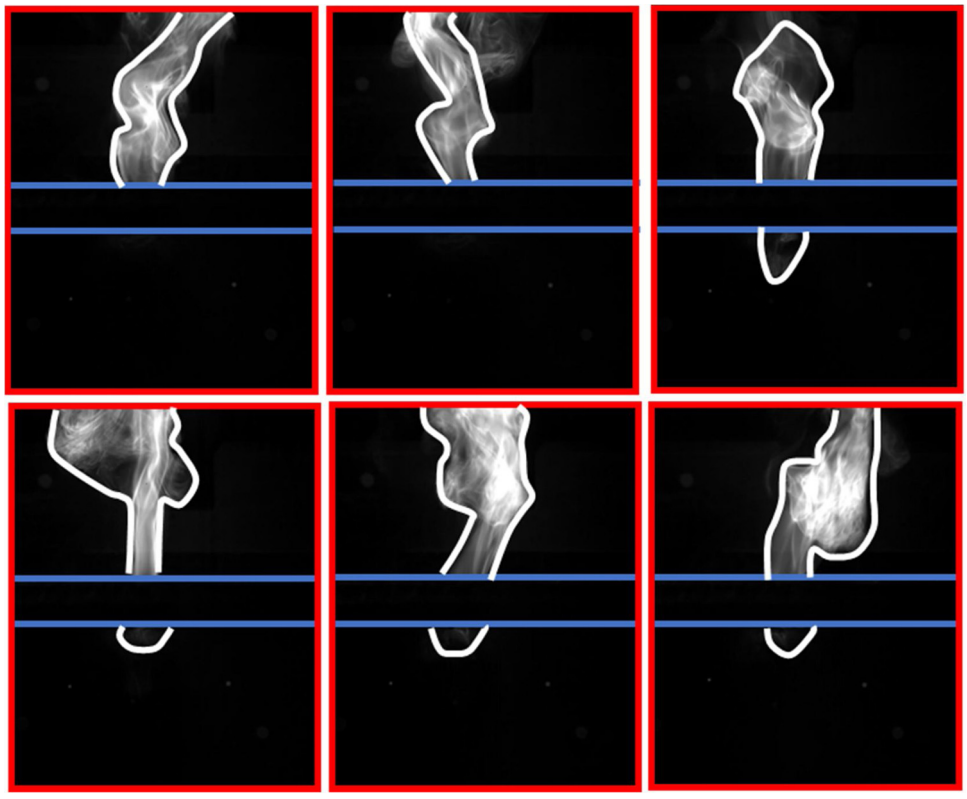

Fig. 14. Time-dependent plasma behavior using novel LSW when laser beam just partially penetrated through the metal sheets. This corresponds to sample 6 in Table 2.

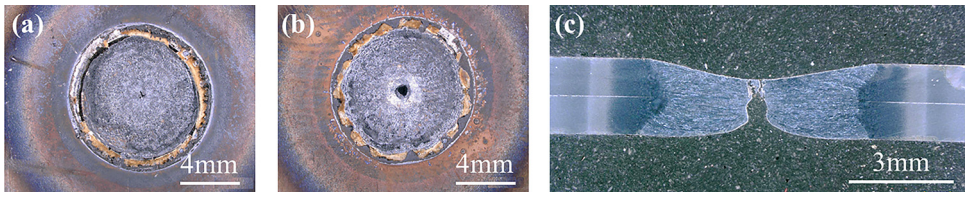

Fig. 15. Typical weld morphology with the welding parameters of sample 6 in Table 2: (a) top view of the weld; (b) bottom view of the weld; (c) cross-sectional view of the weld.

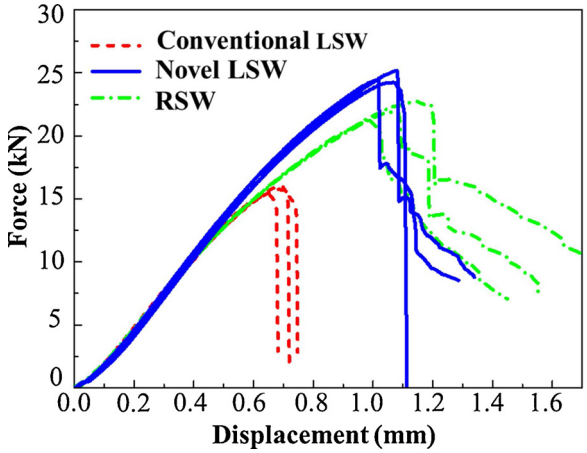

Fig. 16. Comparison of tensile-shear force of the welds obtained by conventional LSW, novel LSW and RSW.

newly developed process was indicated in Fig. 10. Changing laser focus position was realized by varying laser head position driven by the robot. The focus position on the top surface of two metal sheets was defined as reference point. The movement distance, named as *Z*, is positive when focal position was above the top surface. On the contrary, it is negative. All the movements were with a constant moving velocity.

The movement distance, the moving velocity and the corresponding welding duration were indicated in Table 2. As shown in Table 2, the movement distance was set to be ± 10 mm, ± 20 mm and ± 30 mm, respectively and the moving velocity was fixed as 10 mm/s. Therefore, the welding duration was 1 s, 2 s, 3 s, respectively.

Fig. 11 demonstrated the weld diameters at the interface of the welds obtained under different welding parameters corresponding to the samples in Table 2. Compared to the weld diameter obtained by conventional LSW where the laser focal position was set on the top surface and without any movement, the weld diameter at the interface was significantly enlarged when the laser beam was adjusted over time. As shown in Fig. 11, there exists a linear relationship between the movement distance and the weld diameter. In addition, positive movement has higher increase ratio than that with negative movement. For example, when the movement distance was +30 mm, the weld diameter reached to 7.10 mm, 29.1 % larger than that of conventional LSW weld, as shown by the black dash line in Fig. 11. The increased size of the weld diameter could be attributed to the enlarged irradiated area, which facilitates heat transfer to base materials and reduces the loss of laser power energy and materials as conventional LSW.

The high-speed camera was also applied to real-time monitor newly developed LSW process. By analyzing change in the plasma area above top surface and below the bottom surface in Fig. 12, the novel LSW process can be classified by three phases based on their features: (I) before laser beam fully penetrated through the two metal sheets; (II) when laser beam fully penetrated through the bottom of the metal sheets; (III) when laser beam just partially penetrated through the bottom of the metal sheets. Similar to conventional LSW process, the molten pool strongly fluctuates around the laser beam when laser beam did not fully penetrate through the metal sheets. Also, the shape and size of laser-induced plasma and plume were changed over time. As the laser beam fully penetrated through the metal sheets, laser-induced plasma and plume were observed below the bottom of the metal sheets in Fig. 13. Different from the conventional LSW process, the laser-induced plasma and plume under the metal sheets has a similar size as that above the top surface. This phemomena indicates laser beam energy is continuously absorbed, resulting in increase of the weld diameter.

Compared with conventional LSW process, more uniform shape and size of laser-induced plasma and plume above the molten pool were observed in the novel LSW process, as shown in Fig. 14. Furthermore, expulsion was almost disappeared below the bottom of metal sheets. The reason for these phenomena is contributed to reduced laser beam energy density. As laser beam was moved away from the top surface of the metal sheets, the irradiated laser beam area on the top surface was enlarged, thus reducing the laser beam energy density. Gradually reducing laser beam energy density firstly reduced the keyhole depth, then transferred the laser keyhole mode into the conduction mode. As a result, the recoil pressure is also gradually reduced, thus surface tension of liquid metal can hold the liquid metal. This is indirectly approved by dramatically reduced ejection of the liquid metal from the bottom of the metal sheets.

Fig. 15 shows the top, bottom and cross-sectional views of the typical welds obtained by the welding parameter of sample 6. A typical "X-shape" weld morphology was observed, as shown in Fig. 15c. It can be seen that small collapse only occurred on the top surface center due to the loss of the vaporized materials. A shrinkage porosity was also observed at the bottom center of the weld.

3.4. Comparison of the tensile shear strength of the welds obtained by conventional LSW process, novel LSW process and RSW process

To compare the weld performance, the welds were made with same heat input by conventional and novel LSW processes. The specific welding parameters were as follows: a) laser power of 2500 W, welding duration of 3 s with fixed focal position at top surface; b) laser power of

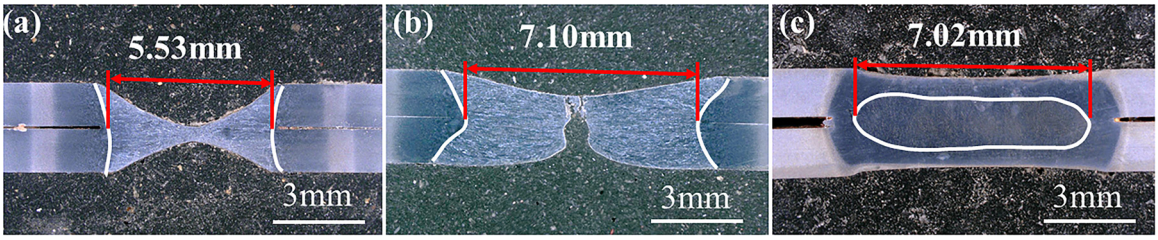

Fig. 17. The weld nugget size of the interface achieved by (a) conventional LSW process; (b) novel LSW process and (c) RSW process.

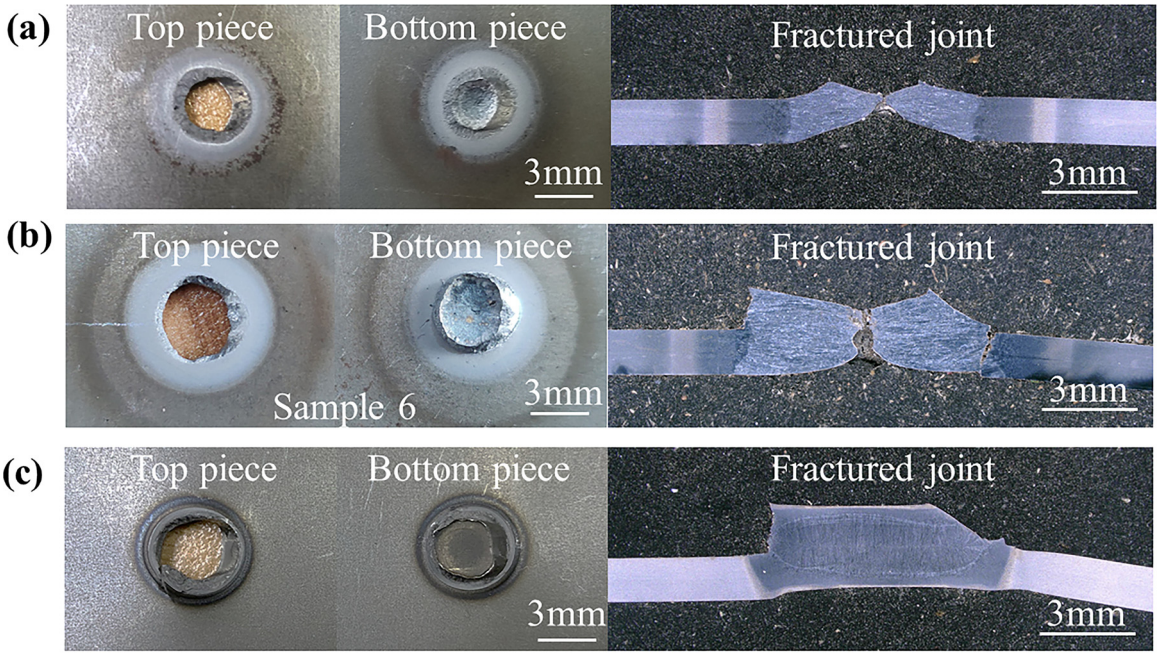

Fig. 18. The fractured joints of the welds obtained by (a) conventional LSW process; (b) novel LSW process and (c) RSW process.

2500 W, welding duration of 3 s, movement distance of +30 mm and moving velocity of 10 mm/s. Furthermore, resistance spot welds were also made for comparison. As shown in Fig. 16, the average tensile shear strength of 24.61 kN was obtained using novel LSW technique. However, the welds produced by conventional LSW process only has the average tensile shear strength of 15.08 kN. Compared to conventional LSW, the tensile shear force was significantly improved by 63.20 % with novel LSW. Fig. 17 shows the cross-sections of the welds obtained by conventional LSW process, novel LSW process and RSW process. The weld size obtained by conventional LSW was about 5.53 mm smaller than that of 7.10 mm by novel LSW process. The weld nugget size is one of the main factors, which significantly affect the tensile shear strength of the welds. The improved tensile shear strength with novel LSW process can be attributed to the enlarged weld nugget size. In order to compare the novel LSW and RSW processes, the weld nugget size should be equivalent to each other in two processes. As shown in Fig. 17, the weld nugget size obtained by novel LSW process was 7.10 mm, which is similar to the 7.02 mm weld nugget size by RSW process. It was also clearly shown in Fig. 16 that the welds obtained by novel LSW process can generate higher peak loads of tensile shear force and more consistency compared to RSW.

Fig. 18 shows the typical fractured welds that were produced by conventional LSW process, novel LSW process and RSW process, respectively. Under the tensile shear force, all welds failed in the partial thickness-partial pullout (PT-PP) mode where the crack propagates from the interface into the fusion zone and part of the mating sheet thickness was removed during separation [4]. It can be seen in Fig. 18 that the welds obtained by novel LSW and RSW have a similar fracture behavior compared to the conventional LSW.

4. Conclusion

In this study, laser spot welding process and resistance spot welding process were used to join the QP steels, a novel laser spot welding method was developed to improve the weld performance of QP joints. The main conclusions can be drawn as follows:

1 It is difficult for conventional LSW process with fixed focus position to produce sufficient weld nugget size in QP steels. A large crater is easily produced in the weld center due to a large amount of expulsion occurred during the welding process.
2 The newly developed LSW process with real-time modulating laser focus position can considerably reduce the formation of expulsion, thus avoiding large crater formation in the weld center. The weld nugget size is dramatically increased, which improves the weld strength by 63.2 % compared to conventional LSW. The reason for the improved weld nugget size and the weld strength are the enlarged irradiation area and reduction in lost materials with the increased laser spot size and reduced recoil pressure.
3 Different from conventional LSW process, heat transfer mode for the newly-developed LSW process is the combination of deep keyhole mode and heat conduction mode. At the beginning of novel LSW process, it is in deep keyhole mode. With increased movement distance leading to large laser spot size on the top surface, heat transfer is switched to heat conduction mode.
4 The novel LSW process can produce comparable weld nugget size and weld strength as RSW process. The average peak load of the tensile shear strength for novel LSW weld is 24.61 kN, which is higher than 21.99 kN of RSW weld.

Declaration of Competing Interest

The authors declare that they have no known competing financial interests or personal relationships that could have appeared to influence the work reported in this paper.

Acknowledgment

This work was supported by the Chinese Academy of Sciences (NO. 292017312D1100301)

References

[1] Matlock DK, Speer JG, De Moor E, Gibbs PJ. Recent developments in advanced high strength sheet steels for automotive applications: an overview. Jestech 2012;15(1):1–12.
[2] Speer J, Matlock DK, De Cooman BC, Schroth JG. Carbon partitioning into austenite after martensite transformation. Acta Mater 2003;51(9):2611–22. https://doi.org/10.1016/S1359-6454(03)00059-4.
[3] Lopez-Cortez VH, Reyes-Valdes FA. Understanding resistance spot welding of

advanced high-strength steels. Weld J 2008;87(12):36–40.
[4] Pouranvari M, Marashi SPH. Critical review of automotive steels spot welding: process, structure and properties. Sci Technol Weld Joi 2013;18(5):361–403. https://doi.org/10.1179/1362171813Y.0000000120.
[5] Liu XD, Xu YB, Misra RDK, Peng F, Wang Y, Du YB. Mechanical properties in double pulse resistance spot welding of Q&P 980 steel. J Mater Process Tech 2019;263:186–97. https://doi.org/10.1016/j.jmatprotec.2018.08.018.
[6] Russo Spena P, Rossi S, Wurzer R. Effects of welding parameters on strength and corrosion behavior of dissimilar galvanized Q&P and TRIP spot welds. Metals 2017;7(12):534. https://doi.org/10.3390/met7120534.
[7] Zhang HY, Senkara J. Resistance welding: fundamentals and applications. London: Taylor & Francis CRC Press; 2005.
[8] Sharma RS, Molian P. Weldability of advanced high strength steels using an Yb: YAG disk laser. J Mater Process Tech 2011;211(11):1888–97. https://doi.org/10.1016/j.jmatprotec.2011.06.009.
[9] Yang SL, Kovacevic R. Welding of galvanized dual-phase 980 steel in a gap-free lap joint configuration. Weld J 2009;88(8):168–78.
[10] Yang S, Carlson B, Kovacevic R. Laser welding of high-strength galvanized steels in a gap-free lap joint configuration under different shielding conditions. Weld J 2011;90(1):8s–17s.
[11] Yang S, Chen Z, Tao W, Wang C, Wang J, Carlson BE. Semi cutting assisted laser welding of zinc coated steels in a zero root opening, lap joint configuration. Weld J 2014;93(1):331s–7s.
[12] Yang YS, Lee SH. A study on the joining strength of laser spot welding for automotive applications. J Mater Process Tech 1999;94(2–3):151–6. https://doi.org/10.1016/S0924-0136(99)00094-1.
[13] Kaplan AFH, Mizutani M, Katayama S, Matsunawa A. Keyhole laser spot welding. International Congress on Applications of Lasers & Electro-optics. LIA 2002;2002(1):169925https://doi.org/10.2351/1.5066203.
[14] Daneshpour S, Riekehr S, Koçak M, Ventzke V, Koruk AI. Failure behaviour of laser spot welds of TRIP800 steel sheets under coach–peel loading. Sci Technol Weld Joi 2007;12(6):508–15. https://doi.org/10.1179/174329307X213855.
[15] Daneshpour S, Riekehr S, Kocak M, Gerritsen CHJ. Mechanical and fatigue behaviour of laser and resistance spot welds in advanced high strength steels. Sci Technol Weld Joi 2009;14(1):20–5. https://doi.org/10.1179/136217108X336298.
[16] Masoumi M, Marashi SPH, Pouranvari M. Metallurgical and mechanical characterization of laser spot welded low carbon steel sheets. Steel Res Int 2010;81(12):1144–50. https://doi.org/10.1002/srin.201000064.
[17] Shanmugam NS, Buvanashekaran G, Sankaranarayanasamy K. Some studies on weld bead geometries for laser spot welding process using finite element analysis. Mater Design 2012;34:412–26. https://doi.org/10.1016/j.matdes.2011.08.005.
[18] Alizadeh-Sh M, Falsafi F, Masoumi M, Marashi SPH, Pouranvari M. Laser spot welding of AISI 304L: metallurgical and mechanical properties. Ironmak Steelmak 2014;41(3):161–5. https://doi.org/10.1179/1743281213Y.0000000112.
[19] Miyagi M, Kawahito Y, Wang H, Kawakami H, Shoubu T, Tsukamoto M. X-ray phase contrast observation of solidification and hot crack propagation in laser spot welding of aluminum alloy. Opt Express 2018;26(18):22626–36. https://doi.org/10.1364/OE.26.022626.
[20] Zhang X, Cao Z. Effects of pulse shaping on Nd: YAG laser spot welds in an AZ31 magnesium alloy. Opt Lasers Eng 2019;119:1–8. https://doi.org/10.1016/j.optlaseng.2019.02.002.